Angiotensin II receptor blocker improves the lowered exercise capacity and impaired mitochondrial function of the skeletal muscle in type 2 diabetic mice

by Ali Sobirin

Submission date: 18-Sep-2019 09:02AM (UTC+0700)
Submission ID: 1174823960
File name: rial_function_of_the_skeletal_muscle_in_type_2_diabetic_mice.pdf (1.76M)
Word count: 12161
Character count: 59263

J Appl Physiol 114: 844–857, 2013.
First published January 17, 2013; doi:10.1152/japplphysiol.00053.2012.

Angiotensin II receptor blocker improves the lowered exercise capacity and impaired mitochondrial function of the skeletal muscle in type 2 diabetic mice

Shingo Takada,[1,2] Shintaro Kinugawa,[1] Kagami Hirabayashi,[1] Tadashi Suga,[1,2] Takashi Yokota,[1] Masashige Takahashi,[1] Arata Fukushima,[1] Tsuneaki Homma,[1] Taisuke Ono,[1] Mochamad A. Sobirin,[3] Yoshihiro Masaki,[1] Wataru Mizushima,[1] Tomoyasu Kadoguchi,[1] Koichi Okita,[4] and Hiroyuki Tsutsui[1]

[1]*Department of Cardiovascular Medicine, Hokkaido University Graduate School of Medicine, Sapporo, Japan;* [2]*Research Fellow of the Japan Society for the Promotion of Science;* [3]*Faculty of Medicine, Diponegoro University, Semarang, Indonesia; and* [4]*Graduate School of Program in Lifelong Learning Studies, Hokusho University, Ebetsu, Japan*

Submitted 12 January 2012; accepted in final form 14 January 2013

Takada S, Kinugawa S, Hirabayashi K, Suga T, Yokota T, Takahashi M, Fukushima A, Homma T, Ono T, Sobirin MA, Masaki Y, Mizushima W, Kadoguchi T, Okita K, Tsutsui H. Angiotensin II receptor blocker improves the lowered exercise capacity and impaired mitochondrial function of the skeletal muscle in type 2 diabetic mice. *J Appl Physiol* 114: 844–857, 2013. First published January 17, 2013; doi:10.1152/japplphysiol.00053.2012.—NAD(P)H oxidase-induced oxidative stress is at least in part involved with lowered exercise capacity and impaired mitochondrial function in high-fat diet (HFD)-induced diabetic mice. NAD(P)H oxidase can be activated by activation of the renin-angiotensin system. We investigated whether ANG II receptor blocker can improve exercise capacity in diabetic mice. C57BL/6J mice were fed a normal diet (ND) or HFD, and each group of mice was divided into two groups: treatment with or without olmesartan (OLM; 3 mg·kg^{-1}·day^{-1} in the drinking water). The following groups of mice were studied: ND, ND+OLM, HFD, and HFD+OLM (n = 10 for each group). After 8 wk, HFD significantly increased body weight, plasma glucose, and insulin compared with ND, and OLM did not affect these parameters in either group. Exercise capacity, as determined by treadmill tests, was significantly reduced in HFD, and this reduction was ameliorated in HFD+OLM. ADP-dependent mitochondrial respiration was significantly decreased, and NAD(P)H oxidase activity and superoxide production by lucigenin chemiluminescence were significantly increased in skeletal muscle from HFD, which were attenuated by OLM. There were no such effects by OLM in ND. We concluded that OLM ameliorated the decrease in exercise capacity in diabetic mice via improvement in mitochondrial function and attenuation of oxidative stress in skeletal muscle. These data may have a clinical impact on exercise capacity in the medical treatment of diabetes mellitus.

oxidative stress; angiotensin; diabetes; mitochondria; muscle

EXERCISE CAPACITY IS LOWERED in patients with metabolic syndrome and type 2 diabetes (30, 42), which is an independent predictor for mortality (37). The first line in the prevention and treatment of diabetes is lifestyle intervention including physical exercise and diet. However, the lowered exercise capacity might prevent the completion of proper and endurance exercise in patients with type 2 diabetes. To date, pharmacological intervention to specifically improve exercise capacity has not been elucidated.

Lowered exercise capacity has been shown to result from abnormalities in energy metabolism in skeletal muscle (26, 42). Moreover, mitochondrial function was impaired in skeletal muscle from patients with type 2 diabetes (22). We previously reported that exercise capacity was lowered and mitochondrial function was impaired in the skeletal muscle from high-fat diet (HFD)-induced type 2 diabetic mice, which was due to enhanced oxidative stress via the activation of NAD(P)H oxidase (41). The NAD(P)H oxidase-induced enhancement of oxidative stress was also demonstrated in skeletal muscle from patients with type 2 diabetes (31). However, the mechanism for activation of NAD(P)H oxidase has not been determined.

NAD(P)H oxidase activity can be increased by high glucose, insulin, and fatty acid as well as activation of the renin-angiotensin system (RAS) (39). RAS has been shown to be activated in the skeletal muscle of fructose-fed diabetic rats (23). Therefore, the activation of RAS may play an important role also in NAD(P)H oxidase and impaired mitochondrial function, leading to the lowered exercise capacity in HFD-induced type 2 diabetic mice. We thus hypothesized that the ANG II type 1 receptor (AT1R) blocker, olmesartan (OLM), could ameliorate the enhanced oxidative stress and lowered exercise capacity in these mice.

The purpose of the present study was to determine whether *1*) RAS is activated in whole body and/or in skeletal muscle from HFD-induced diabetic mice and *2*) the administration of OLM in these mice can ameliorate impaired mitochondrial function and lowered exercise capacity.

MATERIALS AND METHODS

Experimental animals. Male C57BL/6J mice (10–12 wk of age) were housed in an animal room under controlled conditions on a 12:12-h light-dark cycle. Mice were fed for 8 wk on either normal diet (ND; CE-2; CLEA Japan, Tokyo, Japan) containing 4.2% fat and 54.6% carbohydrate or HFD (HFD1; CLEA Japan) containing 32.0% and 29.4% carbohydrate. Mice were divided into two groups with or without OLM (3 mg·kg^{-1}·day^{-1}) in the drinking water, including 0.1% $NaHCO_3$-0.1% $KHCO_3$. The quantities of water consumed by each mouse, as well as body weight, were monitored every week, and the dose of OLM in drinking water was adjusted. We estimated the dose of OLM consumed by mice, which was in the range of 3.0–3.2 mg·kg^{-1}·day^{-1}. The concentration of OLM in the present study was chosen on the basis of previous studies (33, 43). The present study was performed in the following four groups of mice: *1*) ND (n = 10), *2*) ND+OLM (n = 10), *3*) HFD (n = 10), and *4*) HFD+OLM (n = 10). These assignment procedures were performed using numeric codes to identity the animals. All procedures and animal care were approved by our institutional animal research committee and conformed to the animal care guidelines for the Care

Address for reprint requests and other correspondence: S. Kinugawa, Dept. of Cardiovascular Medicine, Hokkaido Univ. Graduate School of Medicine, Kita-15, Nishi-7, Kita-ku, Sapporo 060-8638, Japan (e-mail: tuckahoe@med.hokudai.ac.jp).

and Use of Laboratory Animals at Hokkaido University Graduate School of Medicine.

Eight weeks after treatment, exercise tests and intraperitoneal glucose tolerance tests were performed. After that, blood samples were collected, all mice were euthanized, and organ weight was measured. Because the amount of hindlimb skeletal muscle samples was limited, they were divided for use in the experiments for mitochondrial O_2 consumption ($n = 15$), and the biochemical assay including superoxide (O_2^-) production ($n = 7$) and NAD(P)H oxidase activity ($n = 9$).

Blood pressure measurements. Systemic blood pressure was measured using the tail-cuff method (BP-98A; Softron, Tokyo, Japan) without anesthesia.

Biochemical measurement and organ weight. After the animals had fasted for 6 h, blood samples were collected from the inferior vena cava before euthanizing under deep anesthesia with tribromoethanol-amylene hydrate (Avertin; 2.5% wt/vol, 10 μl/g ip). Plasma insulin levels were measured by ELISA kit (Morinaga Institute of Biochemical Science, Yokohama, Japan). Total cholesterol, triglyceride, and nonesterified fatty acid (NEFA) were measured by using the Cholesterol E-test, Triglyceride E-test, and NEFA C-test, respectively (Wako Pure Chemical Industries, Osaka, Japan). Plasma renin activity levels were measured using a SensoLyte 520 Renin Assay Kit (AnaSpec, San Jose, CA). Serum angiotensin-converting enzyme (ACE) activity levels were measured in a fluorescence assay using an ACE activity assay kit (Life Laboratory, Yamagata, Japan). Plasma ANG II levels were measured using an EIA kit (Peninsula Laboratories, San Carlos, CA). Serum aldosterone levels were measured using an ELISA kit (Endocrine Technologies, Newark, CA). Serum β-hydroxybutyrate (β-OHB) levels were measured using a commercially available kit (Abcam, Cambridge, MA). Heart, epididymal fat, and unilateral hindlimb skeletal muscle were then excised and weighed. Total hindlimb skeletal muscle was used in all experiments except for fiber type staining.

Intraperitoneal glucose and insulin tolerance test. For glucose or insulin tolerance tests, mice were fasted for 4 h and were given an intraperitoneal injection of glucose (1 mg/g) or human regular insulin (0.5 mU/g) in purified water. Blood samples were repeatedly drawn from the tail vein of the same mice before and 15, 30, 60, 90, and 120 min after the injection. Blood glucose levels were determined using a glucometer (Glutest Ace R; Sanwa Kagaku Kenkyusho, Nagoya, Japan).

Immunoblotting in the skeletal muscle. Immunoblotting was performed as previously described (14, 24). Hindlimb skeletal muscle tissue samples were homogenized in 1× cell lysis buffer (Cell Signaling, Danvers, MA), supplemented with 1× complete protease inhibitor cocktail (Roche, Basel, Switzerland) and 1 mmol/l phenylmethylsulphonic fluoride. After sonification and centrifugation at 15,000 *g* for 10 min at 4°C, the supernatants were collected. Protein aliquots were taken for total protein assay (Pierce BCA, Rockford, IL), and the remaining lysate of 20 μg was added onto 10% polyacrylamide gels (Bio-Rad, Hercules, CA), electrophoretically separated by SDS-PAGE using running buffer, and transferred by electroblotting to a polyvinylidene fluoride membrane (Bio-Rad) using transfer buffer at 20 V overnight. After the membranes were blocked in Tris-buffered saline buffer with 0.1% Tween-20 (TBST) in 5% non-fat dry milk, they were incubated overnight at 4°C with primary antibodies (dilution 1:1,000) against the phosphorylated forms of AMP-activated protein kinase α (AMPKα) Thr-172, total AMPKα, Gαq (Cell Signaling), and AT1R (Santa Cruz Biotechnology, Santa Cruz, CA). After being washed three times in TBST buffer, the membranes were incubated with secondary antibodies conjugated with horseradish peroxidase (dilution 1:5,000; Santa Cruz Biotechnology). The membranes were washed again in TBST and incubated with the chemiluminescence detection reagent in the Amersham ECL Western Blotting Analysis System (GE Healthcare, Chalfont St Giles, United Kingdom) for enhanced chemiluminescence. Equal loading of protein was verified by immunoblotting with GAPDH (Cell Signaling).

Quantitative reverse transcription-polymerase chain reaction. Total RNA was extracted from the hindlimb skeletal muscle in the four groups of mice by using QuickGene-810 (Fujifilm, Tokyo, Japan) according to the manufacturer's instructions. The RNA concentration was measured by photometry at 260 nm (Nanodrop, Peqlab, Erlangen, Germany). RNA purity was determined by measuring the 260/280 and 260/230 absorbance ratios. Purity was also tested and was consistently between the 260/280 absorbance ratio of 1.8 and 2.2 (data not shown). The extracted total RNA (2 μg) was reverse-transcribed to cDNA. cDNA was synthesized with a high capacity cDNA reverse transcription kit (10× reverse transcription 2.0 μl, 25× dNTPs 0.8 μl, 10×

Table 1. *Animal characteristics*

	ND	ND+OLM	HFD	HFD+OLM
Hemodynamic measurements				
n	10	10	10	10
Systolic blood pressure, mmHg	102 ± 1	99 ± 1	100 ± 1	95 ± 2*
Heart rate, bpm	623 ± 40	603 ± 42	644 ± 18	640 ± 11
Body weight and organ weight				
n	10	10	10	10
Body wt, g	31 ± 1	31 ± 1	40 ± 1*	40 ± 1*
Heart wt, mg	116 ± 2	112 ± 3	124 ± 3	121 ± 3
Epididymal fat wt, mg	524 ± 29	553 ± 25	2,067 ± 100*	1,864 ± 62*
Skeletal muscle wt, mg	1,045 ± 29	1,006 ± 27	1,157 ± 32	1,185 ± 31
Quadriceps wt, mg	232 ± 8	229 ± 2	222 ± 4	239 ± 5
Gastrocnemius wt, mg	165 ± 6	165 ± 2	177 ± 4	179 ± 3
Soleus wt, mg	10.3 ± 0.5	10.6 ± 0.3	12.2 ± 0.3	12.7 ± 0.3
Heart wt/TL, mg/mm	5.0 ± 0.1	4.9 ± 0.1	5.2 ± 0.1	5.2 ± 0.1
Epididymal fat wt/TL, mg/mm	105 ± 5	118 ± 7	392 ± 20*	359 ± 24*
Skeletal muscle wt/TL, mg/mm	45 ± 1	46 ± 1	50 ± 1	50 ± 1
Biochemical measurements				
n	8	8	8	8
Fasting glucose, mg/ml	103 ± 6	107 ± 5	248 ± 8*	241 ± 9*
Insulin, ng/ml	0.21 ± 0.02	0.24 ± 0.04	1.07 ± 0.21*	0.77 ± 0.13*
Total cholesterol, mg/dl	74 ± 3	72 ± 3	195 ± 10*	194 ± 15*
NEFA, mEq/l	0.42 ± 0.01	0.41 ± 0.02	0.54 ± 0.03*	0.53 ± 0.04*
Triglyceride, mg/dl	53 ± 6	61 ± 6	88 ± 8	94 ± 20

Data are means ± SE. ND, normal diet; OLM, olmesartan; HFD, high-fat diet; wt, weight, TL, tibial length; NEFA, nonesterified fatty acid. *$P < 0.05$ vs. ND.

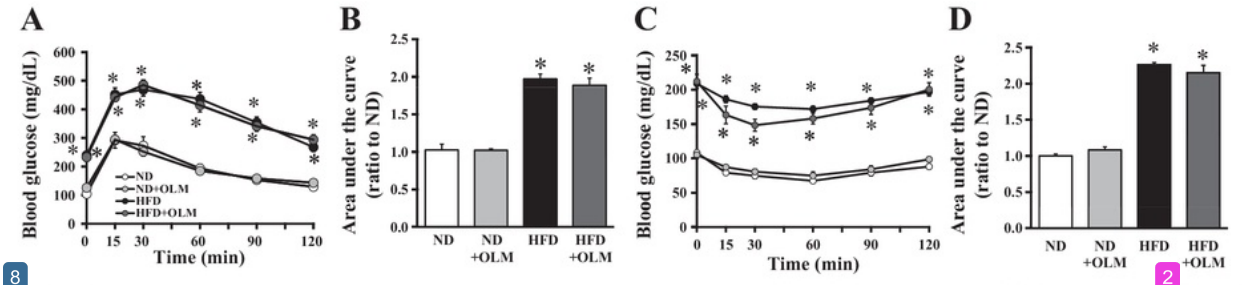

Fig. 1. *A*: blood glucose levels during intraperitoneal glucose tolerance test in the normal diet (ND), ND + olmesartan (OLM), high-fat diet (HFD), and HFD+OLM (n = 10 for each group) mice. *B*: area under the curve of blood glucose levels during intraperitoneal glucose tolerance test in the ND, ND+OLM, HFD, and HFD+OLM mice. *C*: blood glucose levels during intraperitoneal insulin tolerance test in the ND, ND+OLM, HFD, and HFD+OLM mice (n = 8 for each group). *D*: area under the curve of blood glucose levels during intraperitoneal insulin tolerance test in the ND, ND+OLM, HFD, and HFD+OLM mice. Data are means ± SE. Experiments were performed after 8 wk of feeding in all groups. *P < 0.01 vs. ND at each time point.

random primers 1.0 μl, MultiScribe reverse transcription 1.0 μl, RNase inhibitor 1.0 μl, nuclease-free H_2O 3.2 μl; Applied Biosystems, Foster City, CA) using GeneAmp PCR system 2700 (Applied Biosystems). Then 10 μl of diluted RNA samples were mixed with the 10 μl master mix and run on a thermal cycler with the following conditions: *1*) 25°C for 10 min, *2*) 37°C for 120 min, *3*) 85°C for 5 sec, and *4*) 4°C for unlimited time.

TaqMan quantitative PCR was performed with the 7300 real-time PCR system (Applied Biosystems) with the use of the TaqMan Gene Expression Master Mix (Applied Biosystems), 5 ng cDNA, and TaqMan Gene Expression Assays (Applied Biosystems) to amplify samples for angiotensinogen (Mm00599662_m1), cathepsin D (Mm00515586_m1), ACE (Mm00802048_m1), myosin heavy chain (MYH) 1 (MYH1; type IIx fiber, Mm01332489_m1), MYH2 (type IIa fiber, Mm01332564_m1), MYH4 (type IIb fiber, Mm01332518_m1), MYH7 (type I fiber, Mm01319006_g1), citrate synthase (Mm00466043_m1), aconitase 2 (ACO2; Mm00475673_gl), isocitrate dehydrogenase 2 (IDH2; Mm00612429_ml), malate dehydrogenase 2 (MDH2; Mm00725890_s1), ndufa2 (a component of complex I, Mm00477755_g1), uqcrc2 (a component of complex III, Mm00445961_m1), cytochrome *c* (Mm01621048_s1), cox4i1 (a component of complex IV, Mm01250094_ml), peroxisome proliferator-activated receptor gamma coactivator-1α (PGC-1α; Mm01208835_m1), sirt-1 (Mm01168521_ml), mitochondrial transcription factor A (Tfam; Mm00447485_ml), nuclear respiratory factor-1 (NRF-1; Mm01135606_m1), pyruvate kinase m2 (PKm2; Mm00-834102_gH), lactate dehydrogenase b (LDHb; Mm01267402_m1), carnitine palmitoyltransferase-1b (CPT-1b; Mm00487191_g1), fatty acid binding protein 3 (FABP3; Mm02342495_m1), CD36 (FAT/CD36; Mm01135198_m1), fatty acid transport protein 1 (FATP1; Mm00449511_m1), $p22^{phox}$ (Mm00514478_m1), Nox2 (Mm01287743_ml), $p47^{phox}$ (Mm00447921_ml), $p67^{phox}$ (Mm00-726636_ml), $p40^{phox}$ (Mm00476300_ml), Rac-1 (Mm01201653_mH), superoxide dismutase 1 (SOD1; Cu/Zn-SOD, Mm01344233_ml), SOD2 (Mn-SOD, Mm01313000_ml), Cat (Mm00437992), and glutathione peroxidase (GPX; Mm00656767_ml). The real-time PCR detection system (Bio-Rad Laboratories) was used with the following conditions: denaturation at 50°C for 2 min, at 95°C for 10 min, followed by 40 cycles of 95°C for 15 s, and at 60°C for 1 min for annealing and extension. Relative mRNA was analyzed with the delta-delta threshold cycle (ΔΔCt) method and normalized to GAPDH as the internal control. Each ΔCt value was determined by subtracting the GAPDH RNA Ct value from the target gene Ct value. The ΔΔCt value was calculated by subtracting the ΔCt value of the ND mice from the ΔCt value of the ND+OLM, HFD, and HFD+OLM mice. The value $2^{-\Delta\Delta Ct}$ represented the average relative amount of mRNA for each target gene. There was no difference in the GAPDH mRNA Ct value among the four groups of mice. PCR was performed in duplicate.

Treadmill testing with gas analysis. Mice were treadmill tested to measure indexes defining whole body exercise capacity as previously described with minor modification (16, 41). At the time of treadmill testing, each mouse was placed on a treadmill enclosed by a metabolic chamber through which air flow of constant speed (1 l/min) is passing (Oxymax 2; Columbus Instruments, Columbus, OH). O_2 and CO_2 gas fractions were monitored at both the inlet and output ports of the metabolic chamber. Basal measurements were obtained over a period of 10 min. Mice were then provided with a 10-min warm-up period at 6 m/min at zero degrees. After the animals warmed up, the angle was fixed at 10 degrees and the speed was incrementally increased by 2 m/min every 2 min until the mouse reached exhaustion. Exhaustion was defined as spending time (10 s) on the shocker plate without attempting to reengage the treadmill. Whole body O_2 uptake ($\dot{V}O_2$) and CO_2 production ($\dot{V}CO_2$) were automatically calculated every 10 s

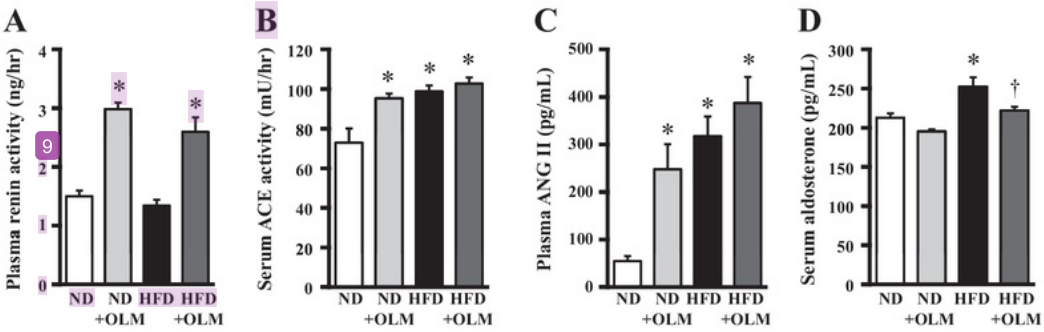

Fig. 2. Summarized data of plasma renin activity (*A*); serum angiotensin-converting enzyme (ACE) activity (*B*); plasma ANG II (*C*); and serum aldosterone (*D*) from 4 groups of ND, ND+OLM, HFD, and HFD+OLM mice. Data are means ± SE. *P < 0.01 vs. ND, †P < 0.01 vs. HFD.

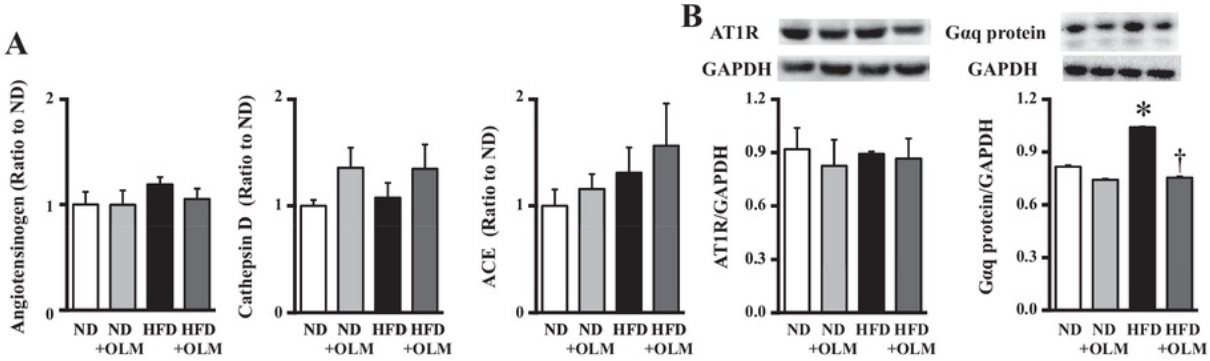

Fig. 3. Summarized data of quantitative analysis of gene expression of angiotensinogen, cathepsin D, and ACE (*A*; $n = 8$ for each group); and ANG II type 1 receptor (AT1R) and Gαq protein (*B*; $n = 6–8$ for each group) in the skeletal muscle from 4 groups of ND, ND+OLM, HFD, and HFD+OLM mice. Gene expression was normalized to GAPDH and depicted as the ratio to ND. Protein expression was normalized to GAPDH. Data are means ± SE. *$P < 0.01$ vs. ND, †$P < 0.01$ vs. HFD.

by taking the difference between the inlet and output gas flow. The respiratory exchange ratio was calculated as $\dot{V}CO_2$ divided by $\dot{V}O_2$. Work was defined as the product of the vertical running distance to exhaustion and body weight.

Blood lactate levels were determined in one drop of blood obtained from tails of mice at rest and at the end of a single bout of exercise by treadmill test. Lactate concentration was assayed using a Lactate Pro-LT portable lactate blood analyzer (Arkray, Kyoto, Japan) according to the manufacturer's instructions.

Spontaneous physical activity. Spontaneous physical activity was measured using an animal movement analysis system (ACTIMO System; Shintechno, Fukuoka, Japan), which consists of a rectangular enclosure (30 × 20 cm), with a sidewall equipped with photosensors at 2-cm intervals (5). Each pair of photosensors scanned animal movement at 0.5-s intervals. Spontaneous activity was recorded after 8 wk in all groups of mice ($n = 8$ each). Mice were placed in individual chambers and housed in cages for 1 day before each recording, to become familiarized with the recording environment. Movement signal counts were performed using the Spike 2 analysis program.

Mitochondrial O_2 consumption in the skeletal muscle. Hindlimb skeletal muscle tissues were quickly harvested, and mitochondria were isolated as previously described (41). The isolated mitochondrial protein concentration was measured by the BCA protein assay (Pierce, Rockford, IL). O_2 consumption by isolated mitochondria was measured polarographically using an O_2 electrode (Yellow Springs Instruments, Yellow Springs, OH) in a closed and magnetically stirred glass chamber at 28°C, as previously described (41). After a 1-min equilibration period, mitochondrial respiration was initiated by the addition of 2.5 mmol/l L-glutamate and L-malate or 10 μmol/l palmitoyl- L-carnitine and 2 mmol/l L-malate as substrates. ADP-stimulated (state 3) respiration was determined after adding ADP (300 μmol/l) (22). The initiation of state 3 was rapidly observed, and concentration of O_2 linearly and sharply declined after the addition of ADP. The cessation of state 3 was also abruptly observed, followed by gentle decline of O_2 concentration with a clear inflection point. Non-ADP-

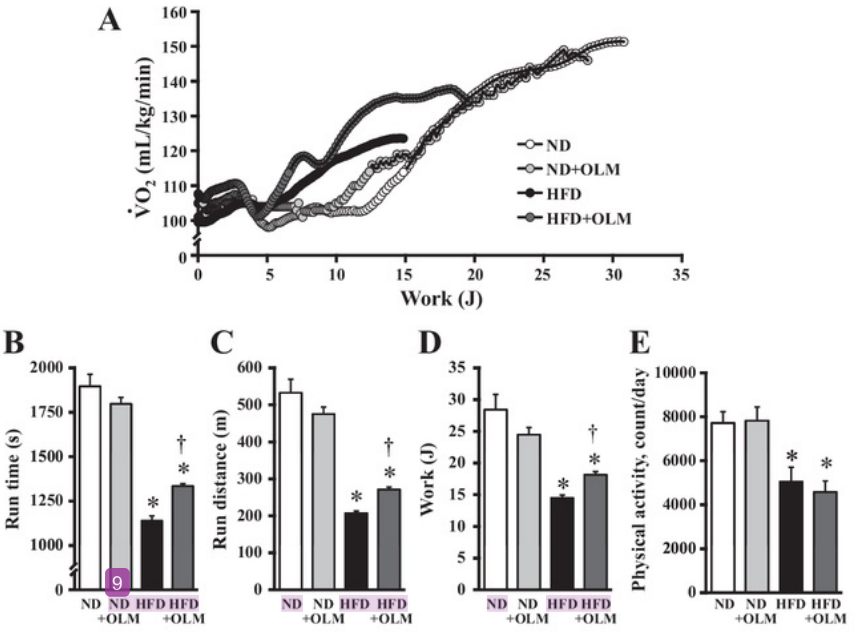

Fig. 4. *A*: representative graphs plotted for O_2 uptake ($\dot{V}O_2$) at each workload during exercise in the ND, ND+OLM, HFD, and HFD+OLM mice. Summarized data of run time (*B*), running distance (*C*), work to exhaustion (*D*), and spontaneous physical activity (*E*) in each group of mice ($n = 10$) are shown. Data are means ± SE. *$P < 0.05$ vs. ND; †$P < 0.05$ vs. HFD.

stimulated (state 4) respiration was measured in the absence of ADP phosphorylation and validated by oligomycin (2 mg/l), an ATPase inhibitor. An inflection point was objectively determined as an intersection point of two regression lines during 30 s after the addition of ADP and 30 s after the addition of oligomycin. The respiratory control index (RCI) was calculated as the ratio of state 3 to state 4 respiration, and the P/O ratio was calculated as the ratio of amount of ATP to consumed O_2 during state 3. Therefore, RCI indicates overall mitochondrial respiratory activity, and P/O ratio indicates efficiency of ATP synthesis.

Mitochondrial membrane potential. Mitochondrial membrane potential in the skeletal muscle was measured by plate reader using the fluorescent probe 5,5′,6,6′-tetrachloro-1,1′,3,3′ tetraethylbenzimidazolylcarbo-cyanine iodide (JC-1; Molecular Probes, Carlsbad, CA). Skeletal muscle cells were loaded with JC-1 for 30 min at 37°C. Samples were excited at 485 nm for monomer fluorescence and 540 nm for JC-1 aggregate fluorescence. Emission fluorescence images were recorded at 560 nm for monomer (green) and 590 nm for JC-1 aggregates (red). The red/green fluorescence ratio was used as an index of changes in membrane potential. Mitochondrial membrane depolarization was indicated by a reduction in the red/green fluorescence intensity ratio. Each experimental group was repeated in duplicate or triplicate wells per plate and averaged to give a single value per experiment.

Histology in skeletal muscle. Hindlimb skeletal muscle was excised, fixed in 4% paraformaldehyde, embedded in paraffin, and stained with hematoxylin-eosin (HE) for histological analysis. Morphological analysis of cell cross-sectional area was performed in at least 50 cells from each mouse (14).

The methods for staining of fiber type have been described previously (11, 29, 40). Gastrocnemius was used in fiber type staining because it consists of a variety of fiber type muscle. In brief, physiological metabolic fiber type designation as slow oxidative, fast oxidative glycolytic, and fast glycolytic is based on cytophotometrically quantified activities of myosin ATPase (marker of contractile activity), succinate dehydrogenase (SDH; marker of oxidative activity), and cyclooxygenase (COX; marker of oxidative activity) in serial cross sections of the same fiber.

Sections were brought to room temperature, air-dried for 30 min, and then stained for ATPase activity following acid (pH 4.51) preincubation. Fiber type classification was performed according to the staining intensities. For determination of ATPase activity, the following procedure was used: preincubation in 50 mmol/l sodium acetate and 30 mmol/l sodium barbital and incubation in 3 mmol/l ATP and 50 mmol/l $CaCl_2$. After they were stained for ATPase activity, sections were processed through 1% $CaCl_2$, 2% $CoCl_2$, and 1% $(NH_4)_2S$ and dehydrated through a graded series of ethanol followed by changes in xylene and then coverslipped.

For SDH, the frozen sections were incubated at 37°C for 30–45 min in a solution containing 1 ml of 0.5 M sodium succinate and 9 ml tetrazolium solution at pH 7. The latter solution contained 2.5 ml nitroblue tetrazolium (2 mg/ml distilled water), 2.5 ml 0.2 M Tris·HCl pH 7.4, 1 ml 0.05 M magnesium chloride, and 3 ml distilled water. Following incubation, the sections were fixed in 15% formol-saline, dehydrated, cleared, and mounted.

COX staining was performed by incubating sections for 1 h in a 50 mM Tris·HCl buffer (pH 7.6) containing 0.22 M sucrose, 14 mM 3,39-diaminobenzidine tetrahydrochloride, 80 mM cytochrome *c*, and 1,300 units catalase. Sites of COX activity were colored brown.

Pyruvate dehydrogenase enzyme activity. Pyruvate dehydrogenase (PDH) enzyme activity was measured using a PDH enzyme activity microplate assay kit according to manufacturer's instructions (MitoSciences, Eugene, OR). In brief, 10 mg of vastus lateralis muscle was homogenized in 100 μl PBS. Sample protein concentration was measured using the Bradford assay before detergent was added to the sample to solubilize intact functional PDH. The samples were then incubated on ice for 10 min before centrifuging at 10,000 *g* for 10 min at 4°C. Sample supernatant was then diluted with buffer to achieve a dilution of 0.2 μg/200 μl; 200 μl of solubilized, diluted sample was added to each well of the microplate before the microplate was incubated for 3 h prior to washing with a stabilizer. Finally, assay solution was added to the plate. before reading the absorbance of each well at 450 nm using a kinetic program with 60 s between reads (Multiskan Ascent plate reader, Ascent software V 2.6; Thermo Scientific, Loughborough, United Kingdom).

O_2^- production, NAD(P)H oxidase activity, thiobarbituric acid reactive substances, and antioxidant capacity. The chemiluminescence elicited by O_2^- in the presence of lucigenin (5 μmol/l) was measured in hindlimb skeletal muscle using a luminometer (AccuFLEX Lumi 400; Aloka, Tokyo, Japan) as previously described (41). To validate that the chemiluminescence signals were derived from O_2^-, the measurements were also performed in the presence of tiron (20 mmol/l), a cell-permeant, nonenzymatic scavenger of O_2^-. NAD(P)H oxidase activity was measured in the homogenates isolated from hindlimb skeletal muscle by the lucigenin assay after the addition of NAD(P)H (300 μmol/l) as previously described (41). In separate experiments, the source of O_2^- production and the role of other enzyme activity for O_2^- production in isolated skeletal muscle from HFD mice were determined. O_2^- production was performed in the absence or presence of various inhibitors, such as rotenone (100 μmol/l), oxyprinol (100 μmol/l), N^G-nitro-L-arginine methyl ester (100 μmol/l), or apocynin (100 μmol/l). Chemiluminescence was also measured in the homogenates isolated from skeletal muscle in HFD mice by the lucigenin assay after the addition of succinate (5 mmol/l), xanthine (100 μmol/l), L-arginine (1 mmol/l), or NAD(P)H (100 μmol/l) (14).

The degree of lipid peroxidation in serum and skeletal muscle was determined though biochemical assay of malondialdehyde formation [tiobarbituric acid reactive substances (TBARS) assay kit; Cayman Chemical, Ann Arbor, MI], according to the manufacturer's protocol, after sonicating for 15 s at 40 V in RIPA buffer [1% (vol/vol) NP-40,

Table 2. *Expired gas analysis and blood lactate analysis*

	ND	ND+OLM	HFD	HFD+OLM
n	10	10	10	10
Peak $\dot{V}O_2$, ml/min	4,537 ± 135	4,218 ± 82	4,553 ± 81	4,839 ± 89
Peak $\dot{V}O_2$/body wt, ml · kg$^-$ · min$^-$	145.3 ± 3.2	143.4 ± 2.1	111.6 ± 1.9*	121.9 ± 2.3*†
Peak $\dot{V}O_2$/skeletal muscle wt, ml · mg$^-$ · min$^-$	4.38 ± 0.21	4.17 ± 0.09	3.83 ± 0.09*	4.24 ± 0.12†
Peak $\dot{V}CO2$, ml/min	4.83 ± 0.17	4.59 ± 0.10	4.91 ± 0.09	5.14 ± 0.10
Peak $\dot{V}CO2$/body wt, ml · kg$^-$ · min$^-$	154.6 ± 3.7	152.2 ± 2.3	119.2 ± 2.0*	129.6 ± 2.8*†
Peak $\dot{V}CO2$/skeletal muscle wt, ml · mg$^-$ · min$^-$	4.77 ± 0.33	4.47 ± 0.07	4.16 ± 0.17	4.47 ± 0.17
Peak respiratory exchange ratio	1.07 ± 0.02	1.07 ± 0.02	1.08 ± 0.02	1.08 ± 0.02
Lactate at rest, mmol/ml	1.9 ± 0.1	1.8 ± 0.1	2.1 ± 0.1	2.0 ± 0.1
Lactate after exercise, mmol/ml	5.7 ± 0.9	7.2 ± 1.0	14.0 ± 0.4*	13.2 ± 0.6*
Lactate after exercise/work, ratio to ND	1.00 ± 0.19	1.49 ± 0.23	5.50 ± 0.15*	3.56 ± 0.13*†

Data are means ± SE. wt, weight; $\dot{V}O_2$, oxygen uptake; $\dot{V}CO2$, carbon dioxide production. *$P < 0.05$ vs. ND; †$P < 0.05$ vs. HFD.

0.5% (wt/vol) sodium deoxycholate, 0.1% (wt/vol) SDS, 0.5 mM phenylmethylsulfonyl fluoride, 0.05 mM Na_3VO_4, 2 mg/ml aprotinin in PBS] with protease inhibitors and centrifuging at 1,600 *g* for 10 min at 4°C. 1,1,3,3,-Tetraehoxypropane was used as standard in this assay.

SOD activity in the skeletal muscle was also measured by enzyme immunoassay (SOD Assay Kit-WST; Dojindo Molecular Technologies, Tokyo, Japan). The SOD Assay Kit-WST assays SOD using WST-1 (2-[4-iodophenyl]-3-[4-nitrophenyl]-5-[2,4-disulfophenyl]-2H-tetrazolium, monosodium salt) that produces a water-soluble formazan dye upon reduction with a superoxide anion. The rate of the reduction with O_2^- is linearly related to xanthine oxidase activity and is inhibited by SOD. The SOD activity was determined by inhibition of the rate of water-soluble formazan formation at 450 nm absorbance.

Cat activities were assayed using the method described in Ref. 20. The reaction mixture (1 ml) consisted of 50 mM potassium phosphate buffer (pH 7.0), 2 M H_2O_2, and a 30-μl sample. The reaction was initiated by the addition of H_2O_2, and absorbance changes were measured at 240 nm (25°C) for 30 s. The molar extinction coefficient for H_2O_2 is 43.6 $M^{-1}cm^{-1}$. Cat activity was expressed as the unit that is defined as millimoles of H_2O_2 consumed per minute per gram of wet tissue.

GPX activity was assayed as described in Ref. 20. The reaction mixtures (1 ml) containing 50 mM potassium phosphate buffer (pH 7.7), 500 mM GSH, 12.5 units GR, 20 mM NADPH, 100 mM NaN_3, 50 mM H_2O_2, and 30-μl samples were incubated at 25°C for 5 min. The kinetic change was spectrophotometrically recorded at 340 nm (25°C) for 3 min. The molar extinction coefficient for H_2O_2 is 66.2 $M^{-1}cm^{-1}$. GPX activity was expressed as a unit, which is defined as the unit (mmol oxidized NADPH/min) per gram of wet tissue.

Statistical analysis. Data are expressed as means ± SE. For multiple-group comparisons, two-way ANOVA followed by the Tukey's test was performed. In intraperitoneal glucose and insulin tolerance tests, differences between groups were determined with repeated-measures ANOVA. A value of $P < 0.05$ was considered statistically significant.

RESULTS

Animal characteristics. Table 1 shows animal characteristics in four groups of mice. There were no significant differences in systolic blood pressure and heart rate between ND and HFD mice.

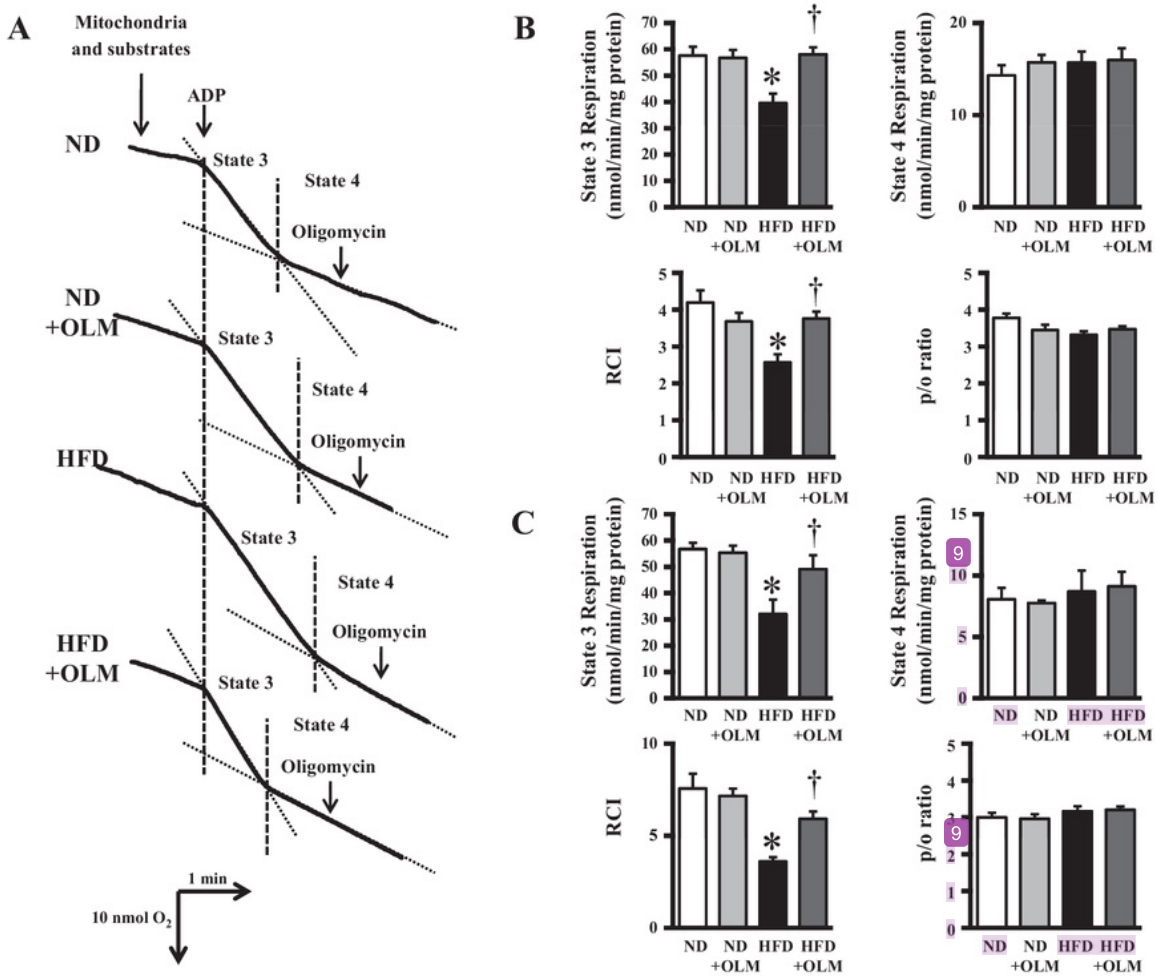

Fig. 5. *A*: representative recordings of ADP-stimulated (state 3) and non-ADP-stimulated (state 4) O_2 consumption in mitochondria isolated from skeletal muscle in the presence of substrates in 4 groups of ND, ND+OLM, HFD, and HFD+OLM mice. Summarized data of state 3 respiration, state 4 respiration, respiratory control index (RCI), and the ratio of ATP amount to consumed O_2 during state 3 (P/O) in glutamate and malate (*B*) and palmitoyl carnitine and malate (*C*) in 4 groups of mice (n = 7–10 for each group) are shown. Data are means ± SE. *$P < 0.05$ vs. ND; †$P < 0.05$ vs. HFD.

Systolic blood pressure in HFD+OLM mice was significantly lower than that in ND mice, but was comparable with that in HFD mice. Heart rate did not change by OLM. Body weight was significantly higher in the HFD mice compared with the ND mice, which was accompanied by the significant increase in epididymal fat weight. There was no difference in the weights of skeletal muscle including quadriceps, gastrocnemius, and soleus between ND and HFD mice. Fasting blood glucose and plasma insulin levels were significantly higher in HFD mice. Total cholesterol and NEFA were also significantly higher in HFD mice, but triglyceride was comparable between ND and HFD mice.

Blood glucose levels during an intraperitoneal glucose and insulin tolerance test were significantly higher in HFD than in ND mice (Fig. 1). These results showed that HFD feeding for 8 wk induced type 2 diabetes with the characteristics of obesity and glucose intolerance. Importantly, HFD+OLM mice showed no significant differences from HFD mice in these parameters (Table 1 and Fig. 1), indicating that OLM did not affect blood pressure, obesity, and diabetic status in HFD.

Blood and skeletal muscle RAS. There was no difference in plasma renin activity between ND and HFD mice, and OLM increased it (Fig. 2*A*). Serum ACE activity and plasma ANG II levels were higher in HFD than in ND mice (Fig. 2, *B* and *C*). OLM significantly increased them in ND mice, and OLM slightly increased them in HFD mice (Fig. 2, *B* and *C*). Serum aldosterone levels were increased in HFD mice compared with ND mice, and significantly decreased in HFD+OLM mice (Fig. 2*D*). We also determined whether RAS in the skeletal muscle was activated. Gene expressions of angiotensinogen, cathepsin D, and ACE were comparable in skeletal muscle among the four groups (Fig. 3, *A*–*C*). There was also no difference in protein levels of AT1R among the four groups (Fig. 3*D*). In contrast, protein levels of Gαq were increased in HFD mice compared with ND mice, and significantly decreased in HFD+OLM mice (Fig. 3*E*).

Exercise capacity. Figure 4*A* shows a representative plot of $\dot{V}O_2$ corresponding to each workload during exercise in ND, ND+OLM, HFD, and HFD+OLM mice. The work to exhaustion was decreased in HFD compared with ND mice, which was accompanied by a decrease in peak $\dot{V}O_2$. These changes were ameliorated in HFD+OLM mice. Run time (Fig. 4*B*), running distance (Fig. 4*C*), and work (Fig. 4*D*) to exhaustion

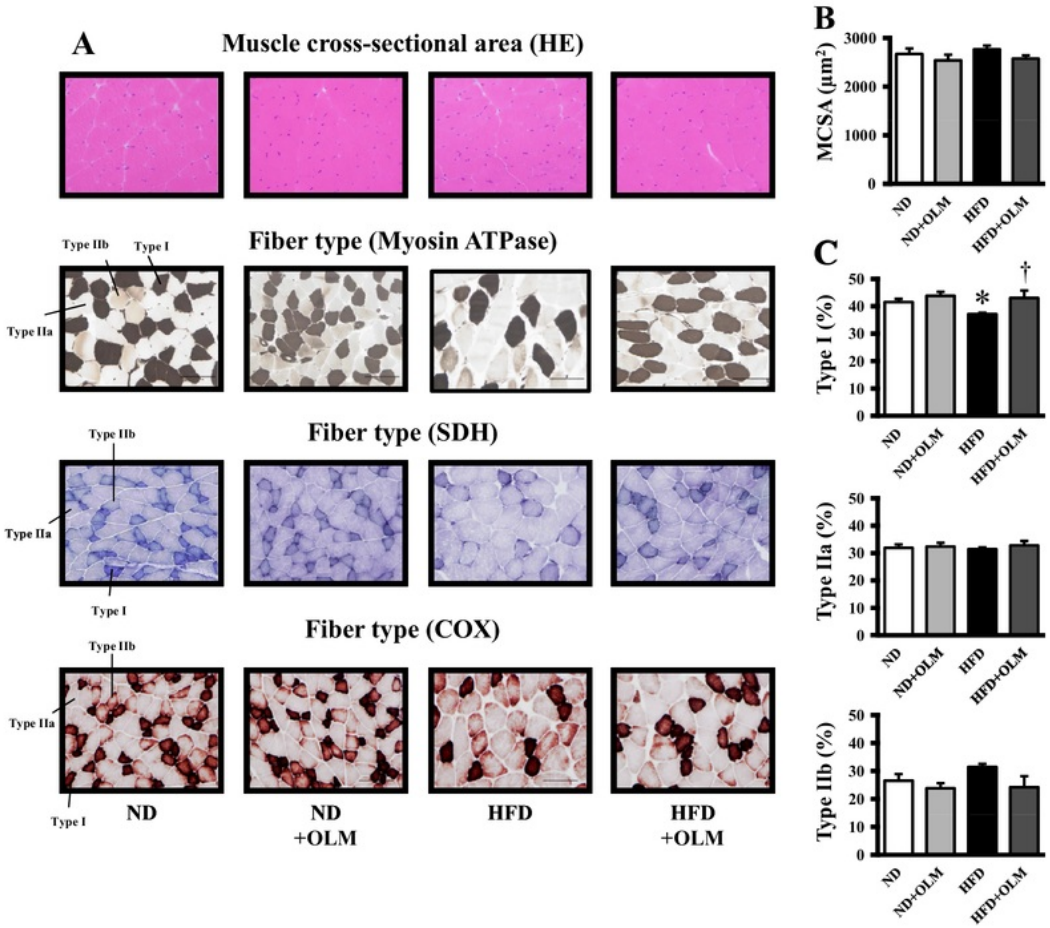

Fig. 6. Representative high-power photomicrographs of skeletal muscle tissue sections stained with hematoxylin-eosin (HE), myosin ATPase, succinate dehydrogenase (SDH), and cyclooxygenase (COX) from 4 groups of ND, ND+OLM, HFD, and HFD+OLM mice (*A*). Scale bar, 100 μm. Summary data of myocyte cross-sectional area (MCSA; *B*) and quantitative analysis of myosin ATPase staining in skeletal muscle obtained from 4 groups of ND, ND+OLM, HFD, and HFD+OLM mice ($n = 3$ for each group; *C*). Data are means ± SE. *$P < 0.05$ vs. ND; †$P < 0.05$ vs. HFD.

were significantly decreased in HFD compared with ND mice and were significantly improved in HFD+OLM mice (respectively, $P < 0.05$). There was no difference in peak $\dot{V}O_2$ and $\dot{V}CO_2$ in either group. Coincident with the limited exercise capacity, peak $\dot{V}O_2$ and $\dot{V}CO_2$ corrected by body weight were significantly decreased in HFD compared with ND mice, and this decrease was ameliorated in HFD+OLM mice (Table 2). Peak respiratory exchange ratio values were >1.0 and did not differ among the four groups of mice, indicating that treadmill tests were performed until exhaustion beyond the anaerobic threshold in all groups of mice. Even after peak $\dot{V}O_2$ was corrected by skeletal muscle weight to exclude the influence of the differences in body composition, it was significantly decreased in HFD compared with ND mice and was significantly improved in HFD+OLM mice (Table 2).

Lactate level at rest was comparable among groups, and lactate level after exercise was increased compared with rest in all groups (Table 2). Lactate level after exercise was significantly increased in HFD mice compared with ND mice and was comparable between HFD and HFD+OLM mice (Table 2). Lactate level corrected by work was significantly decreased in HFD+OLM compared with HFD mice (Table 2).

Spontaneous physical activity. Physical activity was decreased in HFD mice compared with ND mice, and OLM did not affect it in both ND and HFD mice (Fig. 4*E*).

Mitochondrial O_2 consumption in skeletal muscle. Figure 5*A* shows representative recordings of O_2 consumption in mitochondria isolated from hindlimb skeletal muscle measured by O_2 electrodes. RCI was >3.0 in the isolated mitochondria from all ND mice in the present study, indicating that the mitochondria we used was efficient to analyze (4). P/O ratio was 2.5–4.0 in ND mice, and these values were consistent with a previous report (2). P/O ratio is theoretically 2.5 (4), and we could not clarify why the P/O ratio was high. State 3 respiration and RCI were significantly decreased in HFD compared with ND mice without any changes in state 4 respiration in the presence of both glutamate-malate (Fig. 5*B*) and carnitine palmitate-malate (Fig. 5*C*) as substrate. P/O ratio did not differ between groups (Fig. 5, *B* and *C*). HFD+OLM mice had significantly improved state 3 respiration and RCI compared with the HFD mice.

Red/green fluorescence ratio in JC-1 was 2.59 ± 0.17 in mitochondria from ND mice, indicating that membrane integrity was preserved in the isolated mitochondria we used in the present study. Furthermore, it was comparable among ND, ND+OLM, HFD, and HFD+OLM mice (2.59 ± 0.17, 2.51 ± 0.17, 2.26 ± 0.17, and 2.68 ± 0.14, P = not significant).

Fiber type and cell cross-sectional area in skeletal muscle. Figure 6*A* shows representative images of staining for HE, myosin ATPase, SDH, and COX. There was no difference in muscle cell cross-sectional area among the four groups (Fig. 6,

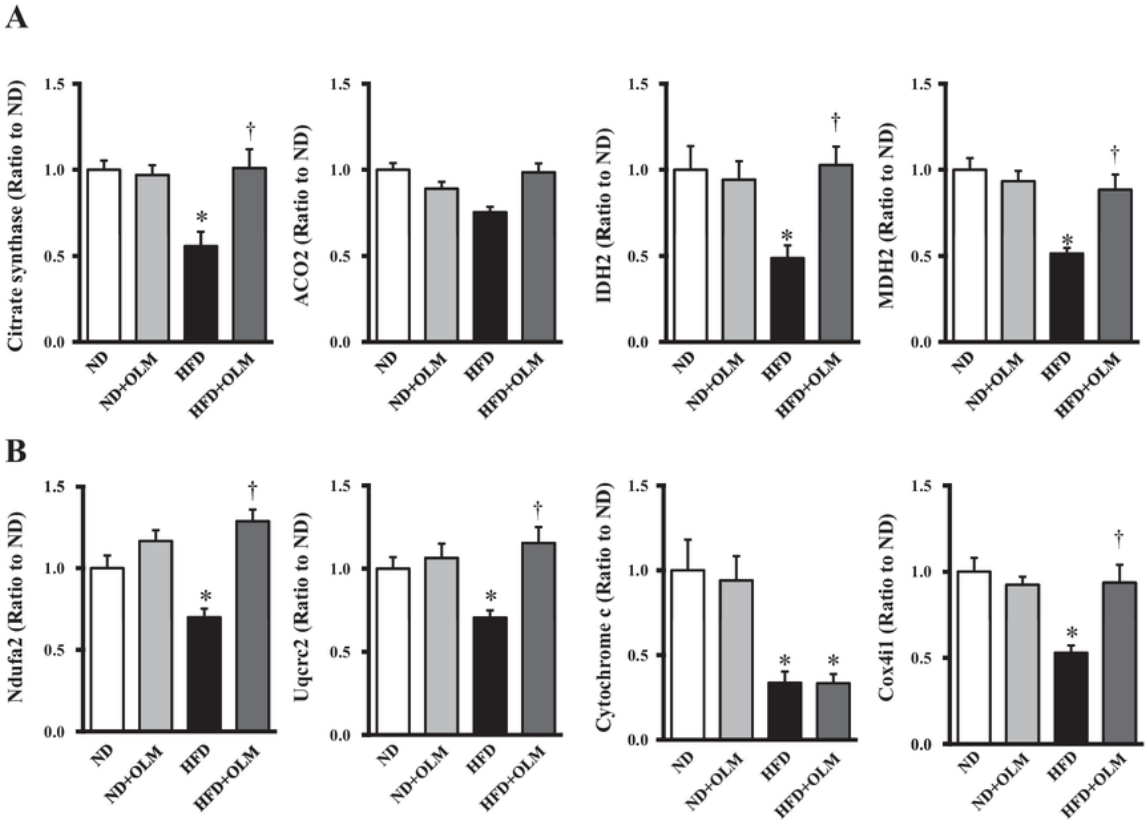

Fig. 7. Quantitative analysis of gene expression of citrate synthase, aconitase 2 (ACO2), isocitrate dehydrogenase 2 (IDH2), and malate dehydrogenase 2 (MDH2) (*A*); and ndufa2, uqcrc2, cytochrome c, and cox4i1 mRNA (*B*) in skeletal muscle obtained from 4 groups of ND, ND+OLM, HFD, and HFD+OLM mice (n = 8 for each group). Data are means ± SE. *$P < 0.01$ vs. ND, †$P < 0.01$ vs. HFD.

A and *B*). Fiber type staining revealed that type I was decreased in HFD mice compared with ND mice, and increased in HFD+OLM mice (Fig. 6*A*). Type IIb was not altered in all groups. Summary data for myosin ATPase staining showed that type I was significantly decreased in HFD mice compared with ND mice, and increased in HFD+OLM mice (Fig. 6*C*). Type IIa and IIb were not altered in all groups (Fig. 6*C*). Gene expressions of MYH2 and MYH7 were significantly decreased in HFD mice compared with ND mice, and increased in HFD+OLM mice (data not shown). MYH1 and MYH4 were not altered in all groups (data not shown).

Gene expressions regulating mitochondrial function and biogenesis. In agreement with the change in O_2 consumption, gene expression of ndufa2, uqcrc2, cytochrome *c*, and cox4i1 was significantly decreased in hindlimb skeletal muscle from HFD compared with ND mice (Fig. 7*A*). Gene expression of citrate synthase, IDH2, and MDH2 was also significantly decreased in HFD compared with ND mice (Fig. 7*B*). Gene expression of ndufa2, uqucr2, cox4i1, citrate synthase IDH2, and MDH2 was significantly improved in HFD+OLM compared with HFD mice (Fig. 7). In contrast, gene expression of PGC-1α, sirt-1, Tfam, and NRF-1 and protein expression of p-AMPK/AMPK were not altered in HFD mice (Fig. 8, *A* and *B*).

Enzyme activity and gene expression regulating glucose and FFA metabolism, and metabolic by-product. PDH activity and gene expression of PKm2 and LDHb were comparable among the four groups (Fig. 9*A*). Serum β-OHB intended to be increased in HFD mice compared with ND mice, and decreased in HFD+OLM mice (Fig. 9*B*). CPT-1b was decreased in HFD mice compared with ND mice, and increased in HFD+OLM mice (Fig. 9*C*). Gene expression of FABP3, CD36 (FAT/CD36), and FATP1 was comparable among the four groups (Fig. 9*C*).

O_2^- production, NAD(P)H oxidase activity, oxidative stress, and gene expression of NAD(P)H oxidase subunits and antioxidant capacity in skeletal muscle. O_2^- production and NAD(P)H oxidase activity measured by lucigenin chemiluminescence were significantly increased in limb skeletal muscle from HFD compared with ND mice, and their changes were inhibited by OLM (Fig. 10, *A* and *B*). Increased O_2^- production in HFD mice was inhibited in the presence of apocynin, and it was not affected in the presence of other inhibitors (Fig. 10*C*). Chemiluminescence signals in the homogenates isolated from skeletal muscle in HFD mice were enhanced by the addition of NAD(P)H, and were not affected by other substrates (Fig. 10*D*). Therefore, these results suggested that the increased O_2^- production in HFD mice was due to increased NAD(P)H oxidase activity, but not mitochondria, xanthine oxidase activity, or nitric oxide synthase activity. TBARS in serum and skeletal muscle were increased in HFD mice compared with ND mice, and were significantly inhibited by OLM (Fig. 10*E*). Gene expression of $p22^{phox}$, $p47^{phox}$, $p67^{phox}$, and $p40^{phox}$ was significantly in-

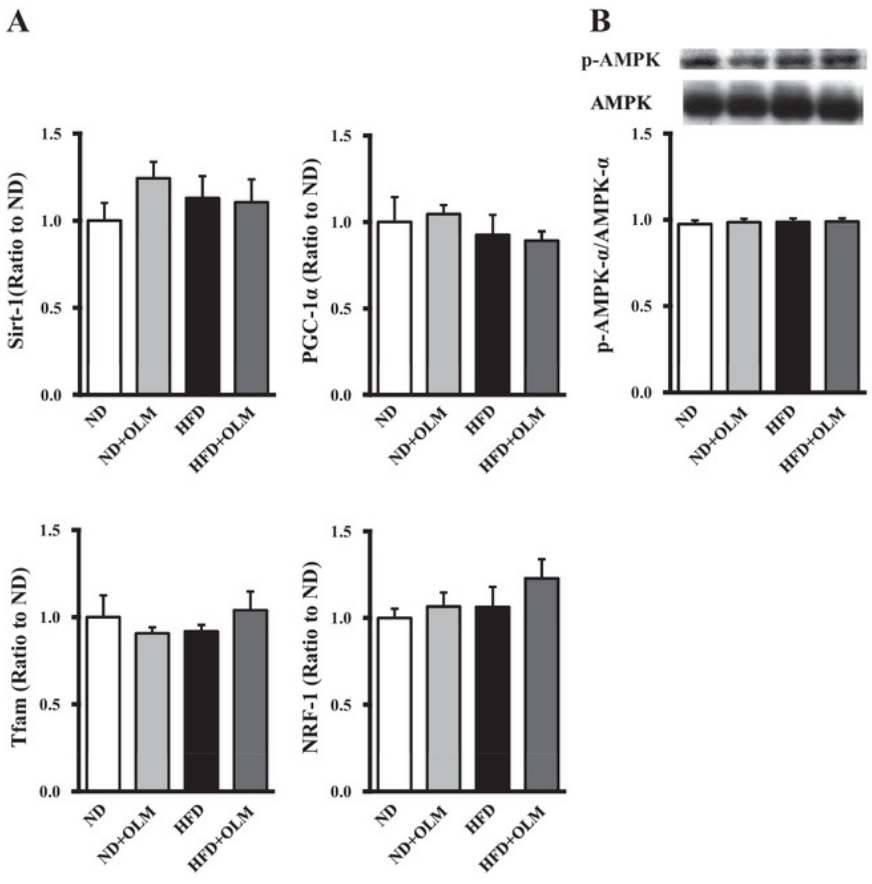

Fig. 8. Summarized data of quantitative analysis of gene expression of sirt-1, peroxisome proliferator-activated receptor gamma coactivator 1α (PGC-1α), mitochondrial transcription factor A (Tfam), and nuclear respiratory factor 1 (NRF-1) mRNA (*A*); and protein level of p-AMP-activated protein kinase (p-AMPK)/AMPK (*B*) in skeletal muscle obtained from 4 groups of ND, ND+OLM, HFD, and HFD+OLM mice ($n = 8$ for each group). Data are means ± SE. *$P < 0.01$ vs. ND, †$P < 0.01$ vs. HFD.

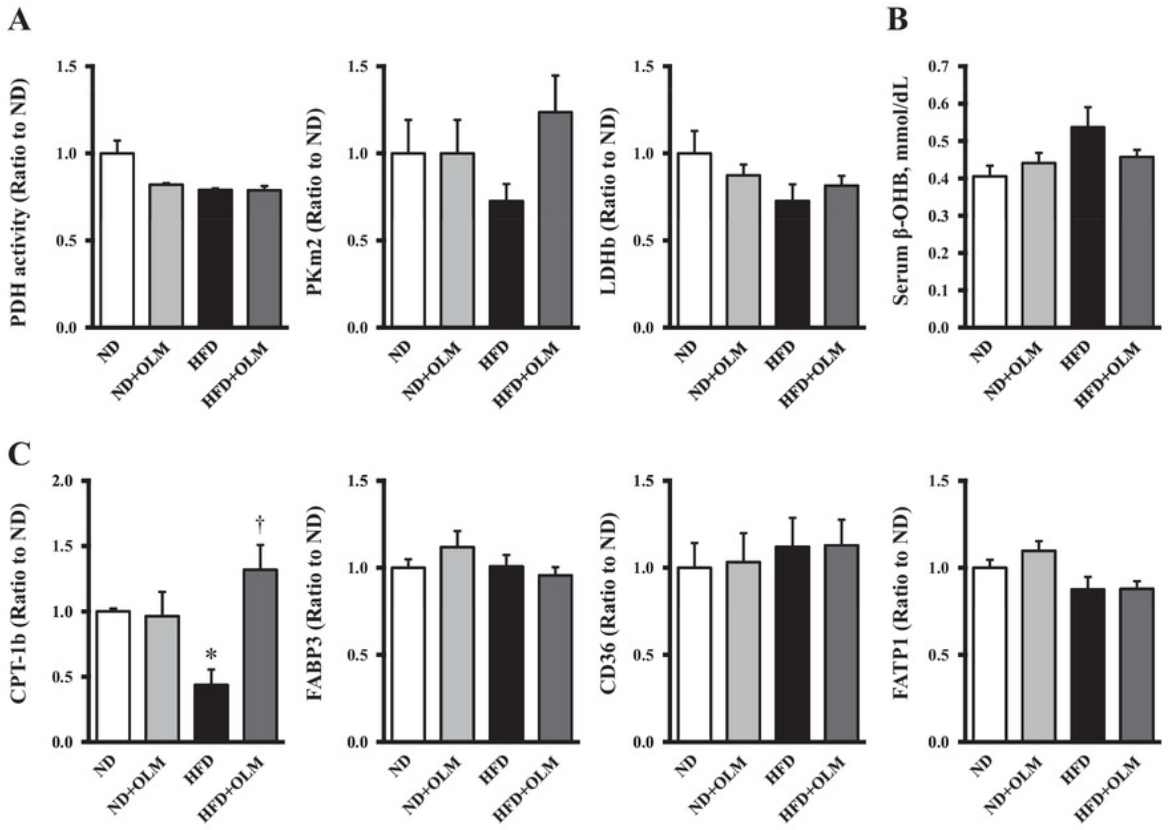

Fig. 9. Summarized data of quantitative analysis of pyruvate dehydrogenase kinase (PDH) activity, gene expression of pyruvate kinase m2 (PKm2), and lactate dehydrogenase b (LDHb) mRNA in skeletal muscle (*A*); serum β-hydroxybutyrate (β-OHB; *B*); and gene expression of carnitine palmitoyltransferase-1b (CPT-1b), fatty acid binding protein 3 (FABP3), CD36 (FAT/CD36), and fatty acid transport protein 1 (FATP1) mRNA (*C*) in skeletal muscle obtained from 4 groups of ND, ND+OLM, HFD, and HFD+OLM mice (n = 8 for each group). Data are means ± SE. *$P < 0.01$ vs. ND, †$P < 0.01$ vs. HFD.

creased in HFD mice compared with ND mice, and improved in HFD+OLM mice (Fig. 10*F*). Gene expression of NOX2 tended to be increased in HFD mice compared with ND mice, which, however, did not reach statistical significance (P = 0.095), and was significantly improved in HFD+OLM mice compared with HFD mice.

SOD, catalase, and GPX activities and gene expressions of SOD1, SOD2, Cat, and GPX were comparable between groups (Fig. 11).

DISCUSSION

HFD-induced type 2 diabetic mice had lowered exercise capacity, a decreased peak $\dot{V}O_2$, impaired mitochondrial respiratory activities, decreased oxidative fiber type, decreased gene expressions of the mitochondrial complex and citrate synthase, and enhanced oxidative stress in skeletal muscle, all of which were significantly ameliorated by chronic treatment of HFD mice with OLM. Therefore, AT1R signaling may be at least in part involved in the lowered exercise capacity and mitochondrial dysfunction of HFD-induced type 2 diabetes.

Activation of RAS in HFD-induced diabetes. The activation of local as well as systemic RAS has been shown to be involved in the development of type 2 diabetes. In a meta-analysis of clinical trials, the inhibitors of RAS have been reported to reduce the new onset of diabetes mellitus (1). In the experimental studies, the treatment with AT1R blocker improved insulin resistance in HFD mice and fructose-fed rats (6, 10, 25). A recent study reported that the expression of AT1R was increased in adipose tissue from HFD mice, which was associated with systemic insulin resistance (6). Furthermore, the activation of RAS, especially local RAS, is also associated with the development of diabetic complications (15, 19, 27). In the present study, serum ACE activity, plasma ANG II level, and serum aldosterone level were increased in HFD mice (Fig. 2). Gene expression of RAS components and AT1R protein level in skeletal muscle did not differ between ND and HFD mice (Fig. 3). In contrast, Gαq protein level in skeletal muscle was increased in HFD mice (Fig. 3). Therefore, these data suggested that systemic RAS and downstream signaling of AT1R in the skeletal muscle were activated in HFD mice.

Beneficial effects of OLM on exercise capacity and mitochondrial function. The most significant finding of the present study is that chronic administration of OLM into HFD mice ameliorated the decrease in exercise capacity (Fig. 4 and Table 2), ameliorated the impaired mitochondrial respiratory function (Fig. 5), improved the decreased oxidative fiber (Fig. 6), and improved the decreased gene expression of mitochondrial complex and tricarboxylic acid (TCA) cycle rate-limiting enzyme

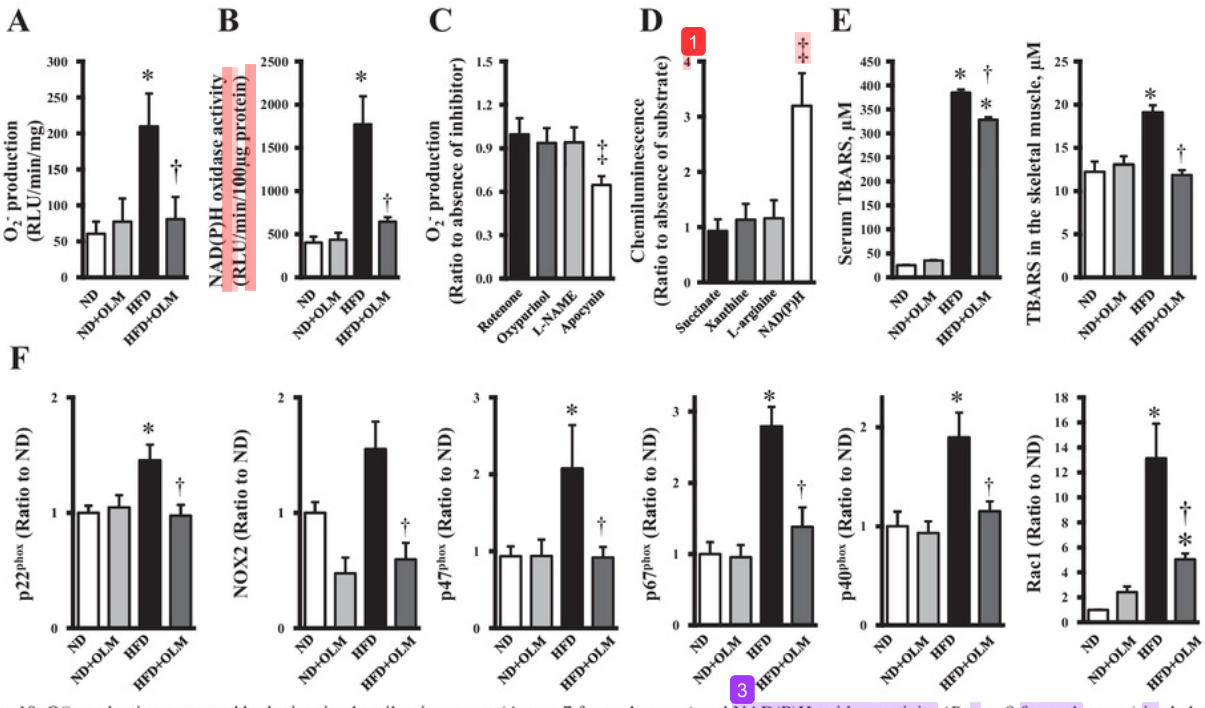

Fig. 10. O_2^- production measured by lucigenin chemiluminescence (*A*; $n = 7$ for each group) and NAD(P)H oxidase activity (*B*; $n = 9$ for each group) in skeletal muscle obtained from 4 groups of ND, ND+OLM, HFD, and HFD+OLM mice. Effects of various inhibitors on O_2^- production (*C*; $n = 6$ for each group) and effects of various substrates on enzymatic activities (*D*; $n = 6$ for each group) in skeletal muscle from HFD are shown. Thiobarbituric acid reactive substance (TBARS) in serum and skeletal muscle (*E*, $n = 5$ for each group), quantitative analysis of gene expressions of NAD(P)H oxidase subunits mRNA ($p22^{phox}$, Nox 2, $p47^{phox}$, $p67^{phox}$, $p40^{phox}$, and rac-1, $n = 8$ for each group; *F*) in skeletal muscle obtained from 4 groups of ND, ND+OLM, HFD, and HFD+OLM mice. Data are means ± SE. RLU, relative light unit; L-NAME, nitro-L-arginine methyl ester. $^*P < 0.05$ vs. ND; $^\dagger P < 0.05$ vs. HFD; $^\ddagger P < 0.05$ vs. absence of inhibitor or substrate.

in the skeletal muscle (Fig. 7). In contrast, OLM did not affect those in ND mice. These results suggested that the activated RAS might be at least in part involved in the lowered exercise capacity in this model. Feng et al. (9) also reported that chronic administration of telmisartan into normal mice enhanced running endurance. However, the enhancement of exercise capacity by telmisartan was associated with the decrease in body weight gain and was considered to be due to the activation of peroxisome proliferator activated receptor δ rather than the inhibition of AT1R in their study. Candesartan has been also demonstrated to improve exercise capacity in patients with hypertension, which, however, was accompanied with the reduction of blood pressure (8). Importantly, the beneficial effects of OLM on exercise capacity shown in the present study were independent of blood pressure, body weight, or glucose metabolism (Table 1 and Fig. 1). However, we could not completely exclude the changes in substrate availability by OLM, because we did not directly measure substrate flux.

Lowered exercise capacity is generally believed to be due to abnormalities in energy metabolism in skeletal muscle (16, 26, 41, 42), which depends on mitochondrial function. Therefore, exercise capacity is closely linked to mitochondrial function in the skeletal muscle. We previously reported that exercise capacity was lowered and mitochondrial function was impaired in ANG II-infused mice, which was associated with enhanced oxidative stress (14). In addition, ANG II has been demonstrated to directly impair mitochondrial function in cultured skeletal muscle cells through the increased production of O_2^- (21). Therefore, based on these our present data also confirmed that AT1R signaling was involved in the lowered exercise capacity and mitochondrial dysfunction in HFD mice.

Mitochondrial function and mitochondrial biogenesis in HFD mice. We observed impaired mitochondrial function including mitochondrial respiratory activity, TCA cycle, and substrate metabolism in HFD mice (Figs. 5, 7, 9). In contrast, there was no difference in gene expressions regulating mitochondrial biogenesis (Fig. 8). PGC-1α is a key factor regulating mitochondrial function as well as fiber type and mitochondrial density. We previously reported that mitochondrial density was decreased in HFD mice compared with ND mice, which was ameliorated by an inhibition of oxidative stress (41). Furthermore, this change in mitochondrial density was consistent with the changes in mitochondrial function and constituents, which agreed with previous reports (7, 13). It has been reported that mitochondrial function and content are impaired through the decreased expression of PGC-1α in C2C12 cells with ANG II and in the skeletal muscle from ANG II-infused mice (21). The differences with our data might be due to the difference in ANG II concentration in animal models (HFD mice with intrinsic RAS activation vs. mice with extrinsic ANG II infusion

Mechanisms for activation of NAD(P)H oxidase in skeletal muscle. The present study demonstrated that oxidative stress was enhanced in skeletal muscle from HFD mice (Fig. 10). It

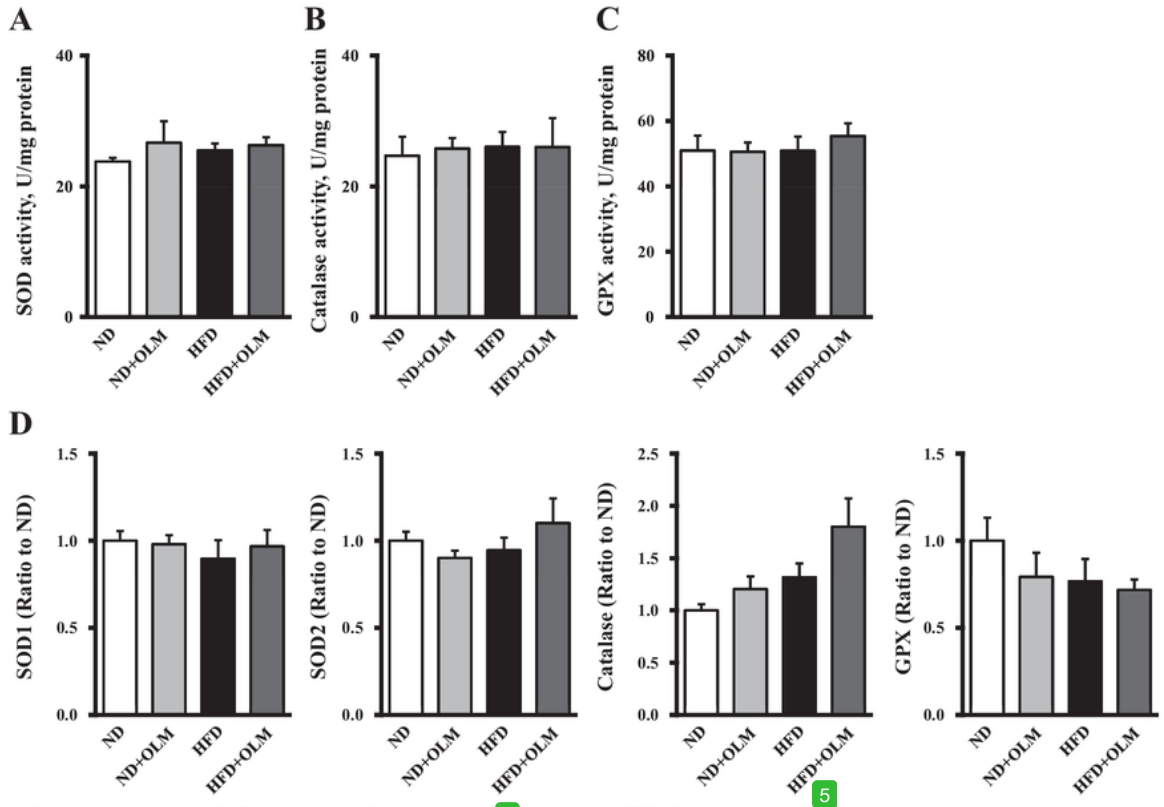

Fig. 11. Superoxide dismutase (SOD; *A*), catalase (*B*), and glutathione peroxidase (GPX; *C*) activity (n = 8 for each group); and quantitative analysis of gene expression of SOD1, SOD2, catalase, and GPX mRNA (*D*; n = 8 for each group) in skeletal muscle obtained from 4 groups of ND, ND+OLM, HFD, and HFD+OLM mice. Data are means ± SE.

has also been confirmed in patients with type 2 diabetes (28) and in an animal model of diabetes (38). Oxidative stress in type 2 diabetes has been shown to be attributable to O_2^- derived from NAD(P)H oxidase (31). Various stimulations, such as high glucose, insulin, and free fatty acids, have been demonstrated to activate NAD(P)H oxidase (39). In the present study, OLM inhibited NAD(P)H oxidase activity and O_2^- production to ND mice levels (Fig. 10). However, it did not affect blood glucose metabolism, plasma insulin, and NEFA (Table 1 and Fig. 1). Therefore, these factors did not participate in the activation of NAD(P)H oxidase in HFD-fed diabetic mice.

ANG II is an important stimulus for NAD(P)H oxidases in a variety of cells, including vascular smooth muscle cells (12), endothelial cells (18), and myocardial cells (32). The activation of AT1R has been reported to lead to c-Src-dependent phosphorylation of $p47^{phox}$ and the subsequent translocation of $p47^{phox}$ to the membrane (35, 36). In addition to the activation of NAD(P)H oxidase, ANG II also increases gene expression of NAD(P)H oxidase subunits. In a cell culture study, ANG II has been shown to upregulate gene expression of the NAD(P)H oxidase subunits Nox2, $p47^{phox}$, $p22^{phox}$, $p67^{phox}$, and $p40^{phox}$ in smooth muscle cells (34). Our data also showed that the gene expression of NAD(P)H oxidase subunits as well as NAD(P)H oxidase activity were increased in skeletal muscle from HFD-fed mice, and OLM completely inhibited this upregulation (Fig. 10).

Limitations. There are several limitations that should be acknowledged in the present study. First, we used only OLM and did not examine the effects of other AT1R blockers. Therefore, we could not comment whether our findings are specific for OLM or other AT1R blockers and could provide similar beneficial effects. Second, OLM did not affect body weight, glucose metabolism, and plasma insulin in HFD-fed mice (Fig. 1 and Table 1). In contrast, previous animal studies have shown that AT1R blocker decreases body weight and plasma insulin and improves glucose metabolism in diabetic models (6, 10, 17, 25). These differences might be due to differences in the species (mice vs. rats) and model (HFD vs. fructose-fed vs. type 2 diabetic KKAy mice) examined, AT1R used (OLM vs. telmisartan vs. valsartan), and the treatment duration (8 wk vs. 12 wk). Finally, OLM completely improved mitochondrial respiration (Fig. 5) and the decreased oxidative fiber (Fig. 6), as well as gene expression levels of oxidative phosphorylation, rate-limiting enzyme of the TCA cycle (Fig. 7), and inhibited oxidative stress (Fig. 10), whereas it partially increased exercise capacity in HFD mice (Fig. 4). These results are consistent with our previous data with apocynin, an inhibitor of NAD(P)H oxidase activation (41). This implies that other mechanisms can also be involved in the lowered exercise capacity in HFD mice. In particular, we could not completely exclude the influence of the increase in body weight and decrease in physical activity on the exercise capacity in HFD mice. How-

ever, these did not affect the favorable effects of OLM on the exercise capacity in HFD mice.

Clinical implication. A drastic increase of patients with type 2 diabetes is a growing medical as well as public health problem in industrialized countries. The lowered exercise capacity in type 2 diabetes could lead to further deterioration of disease by preventing the proper exercise therapy. Our present data showed that the pharmacological treatment to inhibit RAS improved exercise capacity. AT1R blocker is recommended to prevent diabetic complications (3). Therefore, the present study findings may further draw attention to the early and intensive treatment of type 2 diabetes by using AT1R blocker.

CONCLUSION

OLM ameliorated the lowered exercise capacity in HFD-induced diabetic mice via the improvement of impaired mitochondrial function and attenuation of oxidative stress in the skeletal muscle. Treatment with AT1R blocker may attenuate progression in decreased exercise capacity in patients with high risk of type 2 diabetes mellitus.

ACKNOWLEDGMENTS

We thank Kaoruko Kawai for technical assistance and Miwako Fujii and Akiko Aita for biochemical measurements in the experiments.

GRANTS

This study was supported by grants from the Ministry of Education, Science, and Culture (20117004, 21390236, 20590854) and from Daiichi Sankyo Co. Ltd., Japan.

DISCLOSURES

No conflicts of interest, financial or otherwise, are declared by the author(s).

AUTHOR CONTRIBUTIONS

Author contributions: S.T., K.H., T.S., M.T., A.F., T.H., T.O., M.A.S., and T.K. performed experiments; S.T., T.S., M.T., A.F., T.H., and T.O. analyzed data; S.T. and Y.M. prepared figures; S.T. and S.K. drafted manuscript; S.K. conception and design of research; S.K. interpreted results of experiments; S.K., T.Y., K.O., and H.T. edited and revised manuscript; S.K. and H.T. approved final version of manuscript.

REFERENCES

1. **Abuissa H, Jones PG, Marso SP, O'Keefe JH Jr.** Angiotensin-converting enzyme inhibitors or angiotensin receptor blockers for prevention of type 2 diabetes: a meta-analysis of randomized clinical trials. *J Am Coll Cardiol* 46: 821–826, 2005.
2. **Broderick TL, Haloftis G, Paulson DJ.** L-propionylcarnitine enhancement of substrate oxidation and mitochondrial respiration in the diabetic rat heart. *J Mol Cell Cardiol* 28: 331–340, 1996.
3. **Ceriello A.** New insights on oxidative stress and diabetic complications may lead to a "causal" antioxidant therapy. *Diabetes Care* 26: 1589–1596, 2003.
4. **Chance B, Williams GR.** Respiratory enzymes in oxidative phosphorylation. I. Kinetics of oxygen utilization. *J Biol Chem* 217: 383–393, 1955.
5. **Chikahisa S, Tominaga K, Kawai T, Kitaoka K, Oishi K, Ishida N, Rokutan K, Sei H.** Bezafibrate, a peroxisome proliferator-activated receptors agonist, decreases body temperature and enhances electroencephalogram delta-oscillation during sleep in mice. *Endocrinology* 149: 5262–5271, 2008.
6. **Cole BK, Keller SR, Wu R, Carter JD, Nadler JL, Nunemaker CS.** Valsartan protects pancreatic islets and adipose tissue from the inflammatory and metabolic consequences of a high-fat diet in mice. *Hypertension* 55: 715–721, 2010.
7. **Davies KJ, Packer L, Brooks GA.** Biochemical adaptation of mitochondria, muscle, and whole-animal respiration to endurance training. *Arch Biochem Biophys* 209: 539–554, 1981.
8. **De Rosa ML, Chiariello M.** Candesartan improves maximal exercise capacity in hypertensives: results of a randomized placebo-controlled crossover trial. *J Clin Hypertens* 11: 192–200, 2009.
9. **Feng X, Luo Z, Ma L, Ma S, Yang D, Zhao Z, Yan Z, He H, Cao T, Liu D, Zhu Z.** Angiotensin II receptor blocker telmisartan enhances running endurance of skeletal muscle through activation of the PPAR δ/AMPK pathway. *J Cell Mol Med* 15: 1572–1581, 2010.
10. **Fujisaka S, Usui I, Kanatani Y, Ikutani M, Takasaki I, Tsuneyama K, Tabuchi Y, Bukhari A, Yamazaki Y, Suzuki H, Senda S, Aminuddin A, Nagai Y, Takatsu K, Kobayashi M, Tobe K.** Telmisartan improves insulin resistance and modulates adipose tissue macrophage polarization in high-fat-fed mice. *Endocrinology* 152: 1789–1799, 2011.
11. **Gosker HR, van Mameren H, van Dijk PJ, Engelen MP, van der Vusse GJ, Wouters EF, Schols AM.** Skeletal muscle fibre-type shifting and metabolic profile in patients with chronic obstructive pulmonary disease. *Eur Respir J* 19: 617–625, 2002.
12. **Griendling K, Minieri C, Ollerenshaw J, Alexander R.** Angiotensin II stimulates NADH and NADPH oxidase activity in cultured vascular smooth muscle cells. *Circ Res* 74: 1141–1148, 1994.
13. **Holloszy JO.** Biochemical adaptations in muscle. Effects of exercise on mitochondrial oxygen uptake and respiratory enzyme activity in skeletal muscle. *J Biol Chem* 242: 2278–2282, 1967.
14. **Inoue N, Kinugawa S, Suga T, Yokota T, Hirabayashi K, Kuroda S, Okita K, Tsutsui H.** Angiotensin II-induced reduction in exercise capacity is associated with increased oxidative stress in skeletal muscle. *Am J Physiol Heart Circ Physiol* 302: H1202–H1210, 2012.
15. **Kim JH, Kim JH, Yu YS, Cho CS, Kim KW.** Blockade of angiotensin II attenuates VEGF-mediated blood-retinal barrier breakdown in diabetic retinopathy. *J Cereb Blood Flow Metab* 29: 621–628, 2009.
16. **Kinugawa S, Wang Z, Kaminski PM, Wolin MS, Edwards JG, Kaley G, Hintze TH.** Limited exercise capacity in heterozygous manganese superoxide dismutase gene-knockout mice: roles of superoxide anion and nitric oxide. *Circulation* 111: 1480–1486, 2005.
17. **Kurata A, Nishizawa H, Kihara S, Maeda N, Sonoda M, Okada T, Ohashi K, Hibuse T, Fujita K, Yasui A, Hiuge A, Kumada M, Kuriyama H, Shimomura I, Funahashi T.** Blockade of angiotensin II type-1 receptor reduces oxidative stress in adipose tissue and ameliorates adipocytokine dysregulation. *Kidney Int* 70: 1717–1724, 2006.
18. **Lang D, Mosfer SI, Shakesby A, Donaldson F, Lewis MJ.** Coronary microvascular endothelial cell redox state in left ventricular hypertrophy: the role of angiotensin II. *Circ Res* 86: 463–469, 2000.
19. **Leehey DJ, Singh AK, Alavi N, Singh R.** Role of angiotensin II in diabetic nephropathy. *Kidney Int* 2000: S93–S98, 2000.
20. **Matsushima S, Kinugawa S, Ide T, Matsusaka H, Inoue N, Ohta Y, Yokota T, Sunagawa K, Tsutsui H.** Overexpression of glutathione peroxidase attenuates myocardial remodeling and preserves diastolic function in diabetic heart. *Am J Physiol Heart Circ Physiol* 291: H2237–H2245, 2006.
21. **Mitsuishi M, Miyashita K, Muraki A, Itoh H.** Angiotensin II reduces mitochondrial content in skeletal muscle and affects glycemic control. *Diabetes* 58: 710–717, 2009.
22. **Mogensen M, Sahlin K, Fernström M, Glintborg D, Vind BF, Beck-Nielsen H, Højlund K.** Mitochondrial respiration is decreased in skeletal muscle of patients with type 2 diabetes. *Diabetes* 56: 1592–1599, 2007.
23. **Nagai Y, Ichihara A, Nakano D, Kimura S, Pelisch N, Fujisawa Y, Hitomi H, Hosomi N, Kiyomoto H, Kohno M, Ito H, Nishiyama A.** Possible contribution of the non-proteolytic activation of prorenin to the development of insulin resistance in fructose-fed rats. *Exp Physiol* 94: 1016–1023, 2009.
24. **Ohta Y, Kinugawa S, Matsushima S, Ono T, Sobirin MA, Inoue N, Yokota T, Hirabayashi K, Tsutsui H.** Oxidative stress impairs insulin signal in skeletal muscle and causes insulin resistance in postinfarct heart failure. *Am J Physiol Heart Circ Physiol* 300: H1637–H1644, 2011.
25. **Okada K, Hirano T, Ran J, Adachi M.** Olmesartan medoxomil, an angiotensin II receptor blocker ameliorates insulin resistance and decreases triglyceride production in fructose-fed rats. *Hypertens Res* 27: 293–299, 2004.
26. **Okita K, Yonezawa K, Nishijima H, Hanada A, Ohtsubo M, Kohya T, Murakami T, Kitabatake A.** Skeletal muscle metabolism limits exercise capacity in patients with chronic heart failure. *Circulation* 98: 1886–1891, 1998.
27. **Perkins BA, Aiello LP, Krolewski AS.** Diabetes complications and the renin-angiotensin system. *N Engl J Med* 361: 83–85, 2009.

28. **Ramakrishna V, Jailkhani R.** Oxidative stress in non-insulin-dependent diabetes mellitus (NIDDM) patients. *Acta Diabetol* 45: 41–46, 2008.
29. **Rashed RM, El-Alfy SH, Mohamed IK.** Histochemical analysis of muscle fiber types of rat superior rectus extraocular muscle. *Acta Histochem* 112: 536–545, 2010.
30. **Regensteiner JG, Sippel J, Mcfarling ET, Wolfel EE, Hiatt WR.** Effects of non-insulin-dependent diabetes on oxygen consumption during treadmill exercise. *Med Sci Sports Exerc* 27: 661–667, 1995.
31. **Roberts CK, Barnard RJ, Sindhu RK, Jurczak M, Ehdaie A, Vaziri ND.** Oxidative stress and dysregulation of NAD(P)H oxidase and antioxidant enzymes in diet-induced metabolic syndrome. *Metabolism* 55: 928–934, 2006.
32. **Suematsu N, Tsutsui H, Wen J, Kang D, Ikeuchi M, Ide T, Hayashidani S, Shiomi T, Kubota T, Hamasaki N, Takeshita A.** Oxidative stress mediates tumor necrosis factor-alpha-induced mitochondrial DNA damage and dysfunction in cardiac myocytes. *Circulation* 107: 1418–1423, 2003.
33. **Suzuki J, Iwai M, Li Z, Li JM, Min LJ, Ide A, Yoshii T, Oshita A, Mogi M, Horiuchi M.** Effect of combination of calcium antagonist, azelnidipine, and AT1 receptor blocker, olmesartan, on atherosclerosis in apolipoprotein E-deficient mice. *J Hypertens* 23: 1383–1389, 2005.
34. **Touyz RM, Chen X, Tabet F, Yao G, He G, Quinn MT, Pagano PJ, Schiffrin EL.** Expression of a functionally active gp91phox-containing neutrophil-type NAD(P)H oxidase in smooth muscle cells from human resistance arteries: regulation by angiotensin II. *Circ Res* 90: 1205–1213, 2002.
35. **Touyz RM, Schiffrin EL.** Ang II-stimulated superoxide production is mediated via phospholipase D in human vascular smooth muscle cells. *Hypertension* 34: 976–982, 1999.
36. **Touyz RM, Yao G, Schiffrin EL.** c-Src induces phosphorylation and translocation of p47phox: role in superoxide generation by angiotensin II in human vascular smooth muscle cells. *Arterioscler Thromb Vasc Biol* 23: 981–987, 2003.
37. **Wei M, Gibbons LW, Kampert JB, Nichaman MZ, Blair SN.** Low cardiorespiratory fitness and physical inactivity as predictors of mortality in men with type 2 diabetes. *Ann Intern Med* 132: 605–611, 2000.
38. **Yamato M, Shiba T, Yoshida M, Ide T, Seri N, Kudou W, Kinugawa S, Tsutsui H.** Fatty acids increase the circulating levels of oxidative stress factors in mice with diet-induced obesity via redox changes of albumin. *FEBS J* 274: 3855–3863, 2007.
39. **Yang M, Kahn AM.** Insulin-stimulated NADH/NAD^+ redox state increases NAD(P)H oxidase activity in cultured rat vascular smooth muscle cells. *Am J Hypertens* 19: 587–592, 2006.
40. **Yasuda K, Nishikawa W, Iwanaka N, Nakamura E, Seino Y, Tsuda K, Ishihara A.** Abnormality in fibre type distribution of soleus and plantaris muscles in non-obese diabetic Goto-Kakizaki rats. *Clin Exp Pharmacol Physiol* 29: 1001–1008, 2002.
41. **Yokota T, Kinugawa S, Hirabayashi K, Matsushima S, Inoue N, Ohta Y, Hamaguchi S, Sobirin MA, Ono T, Suga T, Kuroda S, Tanaka S, Terasaki F, Okita K, Tsutsui H.** Oxidative stress in skeletal muscle impairs mitochondrial respiration and limits exercise capacity in type 2 diabetic mice. *Am J Physiol Heart Circ Physiol* 297: H1069–H1077, 2009.
42. **Yokota T, Kinugawa S, Okita K, Hirabayashi K, Suga T, Hattori M, Nakagawa Y, Oyama-Manabe N, Shirato H, Tsutsui H.** Lower aerobic capacity was associated with abnormal intramuscular energetics in patients with metabolic syndrome. *Hypertens Res* 34: 1029–1034, 2011.
43. **Yuan Z, Nimata M, Okabe T-a, Shioji K, Hasegawa K, Kita T, Kishimoto C.** Olmesartan, a novel AT1 antagonist, suppresses cytotoxic myocardial injury in autoimmune heart failure. *Am J Physiol Heart Circ Physiol* 289: H1147–H1152, 2005.

Angiotensin II receptor blocker improves the lowered exercise capacity and impaired mitochondrial function of the skeletal muscle in type 2 diabetic mice

ORIGINALITY REPORT

22%	17%	25%	%
SIMILARITY INDEX	INTERNET SOURCES	PUBLICATIONS	STUDENT PAPERS

PRIMARY SOURCES

1	ajpendo.physiology.org Internet Source	3%
2	www.atgcchecker.com Internet Source	3%
3	Shouji Matsushima, Shintaro Kinugawa, Takashi Yokota, Naoki Inoue, Yukihiro Ohta, Sanae Hamaguchi, Hiroyuki Tsutsui. "Increased myocardial NAD(P)H oxidase-derived superoxide causes the exacerbation of postinfarct heart failure in type 2 diabetes", American Journal of Physiology-Heart and Circulatory Physiology, 2009 Publication	2%
4	academic.oup.com Internet Source	2%
5	Shingo Takada, Yoshihiro Masaki, Shintaro Kinugawa, Junichi Matsumoto et al. "Dipeptidyl peptidase-4 inhibitor improved exercise capacity	2%

and mitochondrial biogenesis in mice with heart failure via activation of glucagon-like peptide-1 receptor signalling", Cardiovascular Research, 2016
Publication

6	air.unimi.it Internet Source	2%
7	paperity.org Internet Source	1%
8	Yukihiro Ohta, Shintaro Kinugawa, Shouji Matsushima, Taisuke Ono et al. "Oxidative stress impairs insulin signal in skeletal muscle and causes insulin resistance in postinfarct heart failure", American Journal of Physiology-Heart and Circulatory Physiology, 2011 Publication	1%
9	Minji Sohn, Keumji Kim, Md Jamal Uddin, Gayoung Lee, Inah Hwang, Hyeji Kang, Hyunji Kim, Jung Hwa Lee, Hunjoo Ha. "Delayed treatment with fenofibrate protects against high-fat diet-induced kidney injury in mice: the possible role of AMPK autophagy", American Journal of Physiology - Renal Physiology, 2017 Publication	1%
10	Arata Fukushima, Shintaro Kinugawa, Shingo Takada, Junichi Matsumoto et al. "Direct renin inhibitor ameliorates insulin resistance by	1%

improving insulin signaling and oxidative stress in the skeletal muscle from post-infarct heart failure in mice", European Journal of Pharmacology, 2016
Publication

---

11 Koichiro Yasuda. "Abnormality in fibre type distribution of soleus and plantaris muscles in non-obese diabetic Goto-Kakizaki rats", Clinical and Experimental Pharmacology and Physiology, 11/2002
Publication

1%

---

12 Shinji Hagiwara, Tomohito Gohda, Mitsuo Tanimoto, Takamichi Ito et al. "Effects of pyridoxamine (K-163) on glucose intolerance and obesity in high-fat diet C57BL/6J mice", Metabolism, 2009
Publication

1%

---

13 Tiana, L.. "Alterations of Antioxidant Enzymes and Oxidative Damage to Macromolecules in Different Organs of Rats During Aging", Free Radical Biology and Medicine, 199806
Publication

1%

---

14 Rashed M. Rashed, Sherif H. El-Alfy, Ihab K. Mohamed. "Histochemical analysis of muscle fiber types of rat superior rectus extraocular muscle", Acta Histochemica, 2010
Publication

1%

15	onlinelibrary.wiley.com Internet Source	1%
16	www.sbrc.ca Internet Source	1%

Exclude quotes	On	Exclude matches	< 1%
Exclude bibliography	On		